

Geophysical Research Letters

RESEARCH LETTER

10.1029/2019GL082536

Key Points:

- We model wind-driven ionospheric dynamo currents and resulting magnetic fields on the Martian surface
- Surface fields of tens to up to 100 nT are predicted during the day, strongest in the late morning and near solstices and perihelion
- Mars' dynamic dayside magnetic field draping leads to significant daily variability in expected strength and direction of surface fields

Supporting Information:

- Supporting Information S1
- Figure S1
- Data Set S1

Correspondence to:

R. J. Lillis,
rlillis@ssl.berkeley.edu

Citation:

Lillis, R. J., Fillingim, M. O., Ma, Y., Gonzalez-Galindo, F., Forget, F., Johnson, C. L., et al. (2019). Modeling wind-driven ionospheric dynamo currents at Mars: Expectations for InSight magnetic field measurements. *Geophysical Research Letters*, 46, 5083–5091. <https://doi.org/10.1029/2019GL082536>


Received 19 FEB 2019

Accepted 24 APR 2019

Accepted article online 29 APR 2019

Published online 21 MAY 2019

Modeling Wind-Driven Ionospheric Dynamo Currents at Mars: Expectations for InSight Magnetic Field Measurements

Robert J. Lillis¹ , Matthew O. Fillingim¹ , Yingjuan Ma² , Francisco Gonzalez-Galindo³ , François Forget⁴, Catherine L. Johnson^{5,6}, Anna Mittelholz⁵ , Christopher T. Russell² , Laila Andersson⁷ , and Christopher M. Fowler¹ 

¹Space Sciences Laboratory, University of California, Berkeley, CA, USA, ²Department of Earth and Space Sciences, University of California, Los Angeles, CA, USA, ³Instituto de Astrofísica de Andalucía, Granada, Spain, ⁴Laboratoire de Météorologie Dynamique, Paris, France, ⁵Department of Earth, Ocean and Atmospheric Sciences, The University of British Columbia, Vancouver, British Columbia, Canada, ⁶Planetary Science Institute, Tucson, AZ, USA, ⁷Laboratory for Atmospheric and Space Physics, University of Colorado Boulder, Boulder, CO, USA

Abstract We model expected dynamo currents above, and resulting magnetic field profiles at, InSight's landing site on Mars, including for the first time the effect of electron-ion collisions. We calculate their diurnal and seasonal variability using inputs from global models of the Martian thermosphere, ionosphere, and magnetosphere. Modeled currents primarily depend on plasma densities and the strength of the neutral wind component perpendicular to the combined crustal and draped magnetic fields that thread the ionosphere. Negligible at night, currents are the strongest in the late morning and near solstices due to stronger winds and near perihelion due to both stronger winds and higher plasma densities from solar EUV photoionization. Resulting surface magnetic fields of tens of nanotesla and occasionally >100 nT may be expected at the InSight landing site. We expect currents and surface fields to vary significantly with changes in the draped magnetic field caused by Mars' dynamic solar wind environment.

Plain Language Summary In the upper atmospheres of planets, solar extreme ultraviolet (EUV) radiation produces ions and electrons. Electric currents flow whenever electrons and ions move differently from each other, due to their opposite charges and different masses. When neutral wind causes this differential motion, it is called a dynamo current. Here we simulate these dynamo currents above the NASA InSight Mars lander, resulting from magnetic and collision forces acting upon ions and electrons in the Martian upper atmosphere. We find that modeled currents primarily depend on (a) the density of electrons and ions and (b) the strength of the neutral wind component that is perpendicular to the combined draped and crustal magnetic field that sits within the Mars ionosphere. Negligible at night, predicted currents are the strongest in the late morning and near solstices, due to stronger winds, and near Mars' closest approach the sun, due to both stronger winds and higher plasma densities from solar EUV photoionization. Resulting surface magnetic fields of tens of nanotesla and occasionally >100 nT may be expected at the landing site. We expect currents and surface fields to vary significantly with changes in the draped magnetic field caused by Mars' dynamic solar wind and space weather environment.

1. Introduction

1.1. Dynamo Currents

Dynamo currents are an intrinsic feature of planetary ionospheres. They arise from the differential motions of electrons and ions, in the presence of a magnetic field, that result as the two populations respond differently to the same set of forces. Collision and Lorentz forces usually dominate at altitudes where the most plasma exists to supply currents (Heelis, 2004). For the case of Venus, Earth, or Mars and starting in the upper mesosphere (say 60 km), the motion of electrons and ions is dominated by collisions with neutrals, that is, electron and ion winds are essentially identical to neutral winds, and hence, regardless of the availability of plasma, current flow is negligible. However, as altitude increases, the collision frequency with neutrals decreases, and gyromotion around magnetic field lines becomes relatively more important. Since electron gyrofrequencies are ~50,000 times higher than ion gyrofrequencies for a common ion such as

O_2^+ (Mars' dominant ionospheric ion), the critical altitude above which gyromotion dominates over collisions is many scale heights lower for electrons than for ions. The region in between the electron and ion critical altitudes is known as the dynamo region. Here electrons gyrate around magnetic field lines more frequently than they collide with neutrals or ions; they are said to be "magnetized." Ion motion, however, is still dominated by collisions with neutrals and hence by neutral winds. This differential motion of oppositely charged particles is called a dynamo current. At still higher altitudes, collisions become negligible, and the Lorentz force is typically considered the dominant force acting on the plasma. In this case, electrons and ions drift together, and current flow reduces again.

1.2. Earth Versus Mars

The degree of overlap between the altitude ranges of (a) the dynamo region (i.e., where conditions allow currents to flow) and (b) the photo-produced ionosphere (i.e., where sufficient plasma density exists) determines the magnitude of currents that flow, whereas the neutral wind circulation and geometry and topology of magnetic fields determine the directions and patterns of those currents. In this regard, Earth and Mars are very different, largely because of their different magnetic environments. The dynamo region occurs at much higher neutral densities (lower altitudes) on Earth due to the strong dipolar magnetic field ($|B| \sim 10^5$ nT), spanning 70–120 km, partially overlapping with Earth's *E* region (90–150 km) and well below the main *F* layer (>200 km). In contrast, Mars' dayside ionosphere has much weaker fields (a 30–50 nT dominantly horizontal induced field and localized crustal fields up to 1,000 nT; e.g., Brain et al., 2003). Thus, the dynamo occurs at lower neutral densities (higher altitudes), starting around 110–120 km up to 180–200 km and therefore overlapping significantly in altitude with the main M2 layer of the ionosphere (e.g., Withers et al., 2012), enabling stronger currents to flow than on Earth.

1.3. Prior Work

Withers et al. (2005) first identified the dynamo consequences of Mars' magnetic fields and made rough estimates of current densities. They noted that the magnetic fields produced by currents could be comparable to the "background" magnetic field and hence modify it, unlike at Earth where the global dipole field is too strong to be significantly perturbed. Fillingim et al. (2010) examined the nightside ionosphere where electron precipitation creates localized ionization patches and calculated that winds could drive dynamo current densities as high as $1 \mu A/m^2$, using simple assumptions like a constant neutral wind of 100 m/s, uniform in altitude. Fillingim et al. (2012) also estimated the surface-level magnetic perturbation due to these currents. Opengoorth et al. (2010) calculated dayside ionospheric conductivities, which directly relate to ionospheric currents, using an atmospheric model and magnetic field data from Mars Global Surveyor down to 100-km altitude. These studies commented on the double-peaked nature of the Pedersen conductivity, and thus Pedersen current, profiles at Mars in contrast to Earth. Rioussset et al. (2014) addressed the issue of currents modifying fields by conducting a self-consistent multifluid simulation of the complex currents that may flow around idealized crustal dipole and crustal loops due to a uniform neutral wind. Mittelholz et al. (2017) showed that the latitudinal structure and strength of the dayside global external (i.e., noncrustal) field at ~400 km, averaged over the duration of MGS mission, was similar to the field predicted by a simplified model for currents driven by neutral winds, thus suggesting the influence of winds on the Martian ionosphere. More detail on prior work can be found in the recent review by Fillingim (2018).

1.4. Expectations for InSight Fluxgate Magnetometer

The purpose of this study is to use similar methodology (with some improvements) to Fillingim et al. (2010) to calculate expected current patterns in the ionosphere above the InSight lander (Banerdt & Russell, 2017), which landed on Mars on 26 November 2018 carrying the first surface magnetometer (Banfield et al., 2019). Here, instead of making simple, static assumptions about the magnetic field and neutral wind (e.g., Fillingim et al., 2012), we use more realistic assumptions from time-dependent models of Mars' global plasma interaction, ionosphere, and upper atmospheric wind patterns, evaluated above the InSight landing site at Elysium Planitia (135°E, 4.5°N). We predict magnetic field strength and direction at the surface and its diurnal and seasonal variability. Despite the many assumptions made in this study, these predicted magnetic fields should be instructive in interpreting the field InSight measures and helping to understand their origins. At the time of writing, InSight magnetic field data was not yet adequately calibrated nor released publicly, so we present no comparisons.

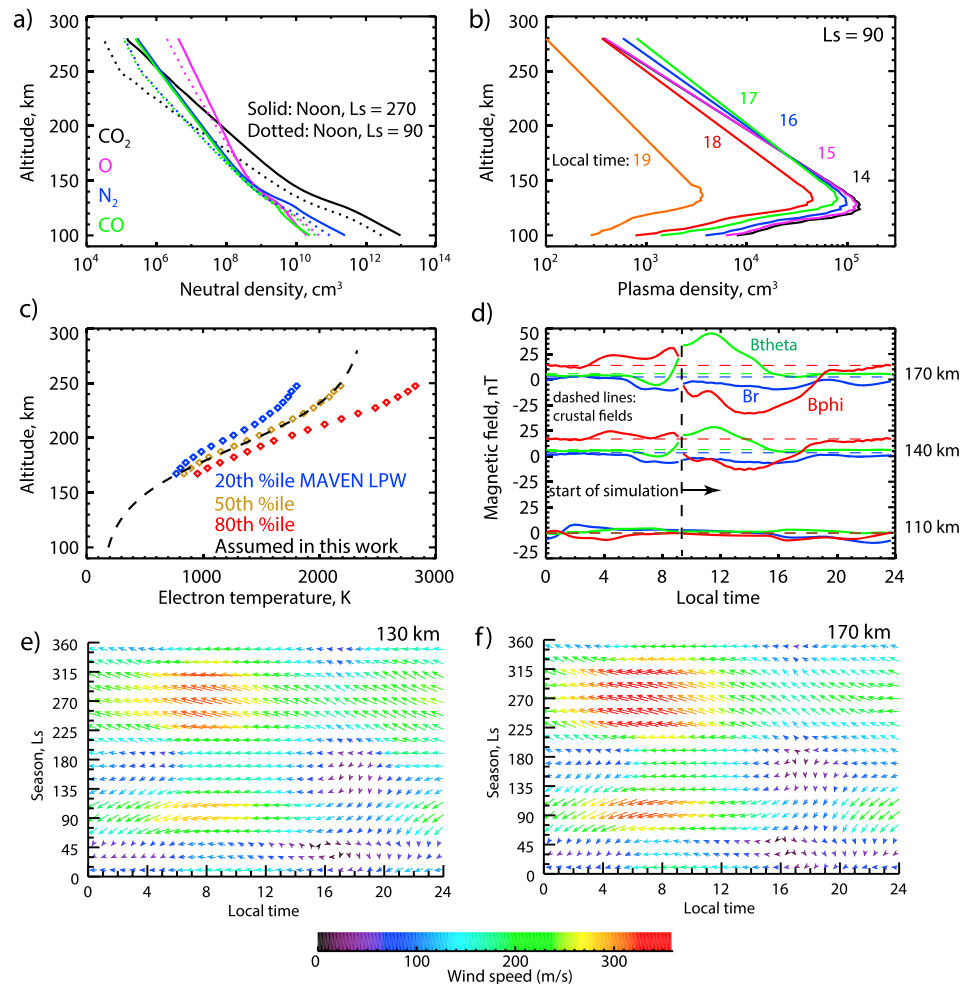


Figure 1. Model inputs used in this study for conditions above the InSight landing site. (a) Neutral densities of the four primary species at northern summer ($L_s = 90^\circ$) and winter solstice ($L_s = 270^\circ$). (b) Plasma densities at several local times at $L_s = 90^\circ$. (c) Electron temperature profile assumed, and dayside measurements made by MAVEN LPW at solar minimum conditions. (d) Magnetic field components in Mars Solar Orbital coordinates at the InSight landing site from the BATS-R-US simulation at three altitudes, starting at 9:30 am. (e and f) Neutral wind vectors at 130- and 170-km altitude as a function of local time and season. Wind vector arrows are as though latitude is on the Y axis. LPW = Langmuir probe/waves.

2. Model Inputs

The inputs to our model are summarized in Figure 1. Neutral densities (Figure 1a), plasma densities (Figure 1b), and neutral winds (Figures 1e and 1f) are taken from the Mars Climate Database v5.3 (Millour et al., 2017), a curated library of simulations of the Martian atmosphere, from ground to exosphere, performed using the Laboratoire Meteorologie Dynamiques Mars Global Circulation Model (LMD-MGCM; Forget et al., 1999; Gonzalez-Galindo et al., 2013). The database is queried for 61 altitudes above the planetary surface (90 km, 92 km, ..., 208 km, 210 km), 37 “seasons” (Solar longitude, $L_s = 0^\circ, 10^\circ, \dots, 350^\circ, 360^\circ$; $L_s = 0^\circ$ corresponds to northern spring equinox), and 73 local times (0:00, 0:20, ..., 23:40, 24:00).

Magnetic fields (Figure 1d) are taken from a time-dependent, multispecies, single-fluid Magnetohydrodynamics (MHD) simulation of the Mars-solar wind interaction using the BATS-R-US model (Ma, 2004; Ma et al., 2017; Ma et al., 2015; validated against Mars Atmosphere and Volatile Evolution (MAVEN) measurements), over one full rotation of the planet while solar wind and interplanetary magnetic field (IMF) conditions were kept constant. Solar wind density, temperature, and velocity were 4 cm^{-3} , 3 eV, and 400 km/s, respectively. The IMF vector was a typical Parker spiral configuration $B_x = 1.634 \text{ nT}$, $B_y =$

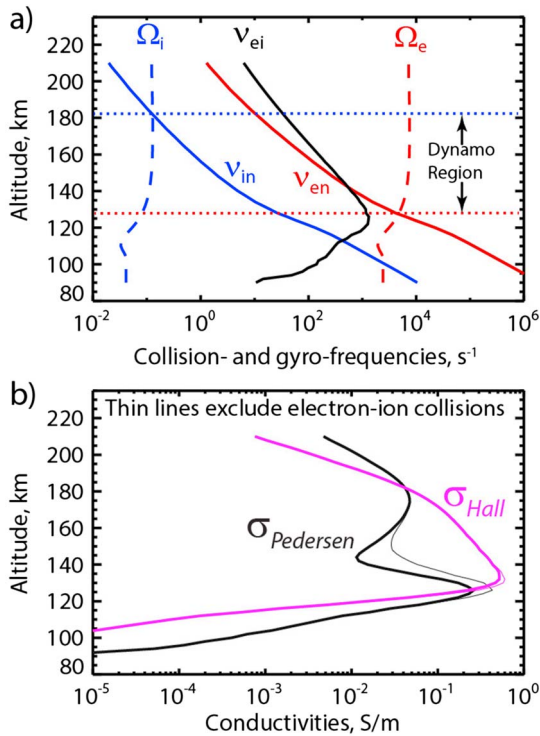


Figure 2. Electrodynamic quantities in the Mars upper atmosphere simulated by the BATS-R-US model and the Laboratoire Meteorologie Dynamiques Mars Global Circulation Model at 14:00 hr local time and $L_s = 0^\circ$. (a) Altitude profiles of gyrofrequencies for electrons and ions (Ω_e , Ω_i) and collision frequencies for ion-neutral (ν_{in}), electron-neutral (ν_{en}), and electron-ion (ν_{ei}) interactions and the resulting dynamo region. (b) Altitude profiles of Hall and Pedersen conductivities. Thin lines show the same quantities ignoring the effects of electron-ion collisions.

-2.516 nT, $B_z = 0$ nT in Mars-Solar-Orbital coordinates. These values are typical for the quiet solar wind conditions seen so far and expected during InSight’s primary mission near solar minimum. The modeled crustal field are primarily eastward, ~ 20 nT at 100 km and decreasing with altitude (Figure 1d). The draped fields across the dayside are largely southwestward, consistent with this IMF orientation, and increase in strength as InSight rotates toward local noon where magnetic pileup is the greatest. Thus, there is a “contest” between the comparable-strength but oppositely-directed crustal and draped fields, resulting in an X line or reconnection point, whose altitude decreases as morning progresses toward noon. Between 9:00 and 10:00, this point decreases rapidly in altitude from above 200 km down to ~ 120 km, causing the field in the ionosphere above InSight to turn rapidly from eastward to southwestward, reaching a maximum just after noon. The draped field then turns westward, weakening as InSight rotates away from the subsolar point. Between 16:00 and 18:00, the reconnection point rises (more slowly than it fell) back above 200 km, and the crustal field direction (east) dominates again as dusk falls and becomes night. This particular run is for solar cycle minimum and spring equinox conditions. For simplicity, we assume these magnetic fields apply to all Mars seasons. It is $\sim 9:30$ a.m. at the InSight landing site at the start of the MHD simulation, hence the discontinuities visible in Figure 1d and later in Figure 4.

Electron temperature is a necessary input to electron-neutral and electron-ion collision frequency formulas (Schunk & Nagy, 2009) but is calculated by neither LMD-GCM nor BATS-R-US. We therefore approximate such profiles by a hyperbolic tangent function (Figure 1c), fit to match the LMD-MGCM neutral temperatures at 100 km and to match average measurements from the MAVEN Langmuir probe/waves experiment (Andersson et al., 2015) at solar minimum conditions, appropriate for InSight’s primary mission. In this work we have only taken horizontal winds from the LMD-MGCM, as vertical winds are typically more than

one order of magnitude smaller (Gonzalez-Galindo et al., 2009). We make the simplifying assumption that the ionosphere is entirely O_2^+ (it accounts for $>90\%$ of the density at these altitudes; Benna et al., 2015) and that electron and ion densities are equal, that is, quasi-neutrality holds.

It is important to note that the magnetic field draping pattern with respect to the neutral wind field will likely play a pivotal role in determining the amplitudes and directions of induced currents. Our assumed upstream solar wind IMF conditions, which directly influence the draping pattern within the ionosphere, are only one example of such conditions.

3. Methodology

For each point in our $61 \times 37 \times 73$ model parameter space of altitudes, seasons, and local times, respectively, we first calculate the important frequencies that define the dynamo region: the gyrofrequencies of electrons (Ω_e) and ions (Ω_i) and the collision frequencies (ion-neutral [ν_{in}], electron-neutral [ν_{en}], and electron-ion [ν_{ei}]). Ion-electron collisions are ignored because the negatively charged electrons can be “pulled” along by the positively charged ions with an efficiency that can be comparable to being “pushed” along by collisions with the moving neutrals, but the electrons “pull” on the much heavier ions is negligible. Collision frequencies are calculated according to Chapter 4 of Schunk and Nagy (2009): ν_{ei} is given by equations 4.57 and 4.140, ν_{in} by equation 4.146 and Table 4.4, and ν_{en} by Table 4.6. These gyrofrequencies and collision frequencies as a function of altitude, for an example case of 14:00 hr local time and $L_s = 0^\circ$ (Figure 2a), show that (a) the dynamo region spans ~ 130 to ~ 185 km and (b) the electron-ion collision frequency (ignored by all previous studies) is comparable to and often exceeds the electron-neutral collision frequency and so should be included.

Having identified the dynamo region, we now calculate the wind-driven currents within this region. Section S1 in the supporting information contains a full derivation of the current vector \mathbf{J}_{wind} as a function of all the properties of the system we are considering: neutral densities and winds, in addition to ion densities and electron densities and temperatures

$$\mathbf{J}_{\text{wind}} = B[\sigma_p \mathbf{U} \times \mathbf{b} + \sigma_h \mathbf{U}^\perp], \quad (1)$$

where vector quantities are bolded, \mathbf{U}^\perp is the component of the neutral wind vector perpendicular to the magnetic field, whose magnitude is B and unit vector is \mathbf{b} , and where σ_p and σ_h are the total Pedersen and Hall conductivities respectively, defined as $\sigma_p = \sigma_{p,e} + \sigma_{p,i}$ and $\sigma_h = \sigma_{h,e} - \sigma_{h,i}$ where $\sigma_{p,e}$, $\sigma_{p,i}$, $\sigma_{h,e}$, and $\sigma_{h,i}$ are the separate electron and ion conductivities:

$$\sigma_{p,i} = Ne^2 \left[\frac{1}{m_i \nu_{in} \left(1 + \frac{\Omega_i^2}{\nu_{in}^2}\right)} - \left(\frac{1}{m_e \nu_{en} \left((1 + \alpha)^2 + \frac{\Omega_e^2}{\nu_{en}^2} \right)} \right) \left(\frac{\alpha + \beta(1 + \alpha)}{1 + \frac{\Omega_i^2}{\nu_{in}^2}} + \alpha \right) \right], \quad (2)$$

$$\sigma_{p,e} = \frac{Ne^2}{m_e \nu_{en}} \left(\frac{1 + \alpha}{(1 + \alpha)^2 + \frac{\Omega_e^2}{\nu_{en}^2}} \right), \quad (3)$$

$$\sigma_{h,i} = \frac{Ne^2 \Omega_i}{\nu_{in} \left(1 + \frac{\Omega_i^2}{\nu_{in}^2}\right)} \left[\frac{1}{m_i \nu_{in}} - \frac{\alpha + \beta(1 + \alpha)}{m_e \nu_{en} \left((1 + \alpha)^2 + \frac{\Omega_e^2}{\nu_{en}^2} \right)} \right], \quad (4)$$

$$\sigma_{h,e} = \frac{Ne^2 \Omega_e}{m_e \nu_{en}^2} \left(\frac{1}{(1 + \alpha)^2 + \frac{\Omega_e^2}{\nu_{en}^2}} \right), \quad (5)$$

where

$$\Omega_i = \frac{eB}{m_i}, \Omega_e = \frac{eB}{m_e}, \quad (6)$$

$$\alpha = \frac{\nu_{ei}}{\nu_{en}}, \beta = \frac{m_e \nu_{ei}}{m_i \nu_{in}}. \quad (7)$$

Here Ω_i and Ω_e are the ion and electron gyrofrequencies, m_i and m_e are the ion and electron masses, e is the electron charge, and N is the total ion and electron density (assumed equal). α and β are dimensionless quantities: α reflects the importance of electron-ion interactions relative to electron-neutral collisions and β the importance of electron-ion interactions to ion-neutral interactions. Note that β is also proportional to the mass ratio of electrons to ions so is typically much smaller than α .

The current equation (1) above may appear unusual to readers familiar with Hall and Pedersen currents in the context of electric fields representing the driving source, where the Pedersen current is perpendicular to the magnetic field and the Hall current is perpendicular to both the magnetic and electric field. However, in this study the driving force is the Lorentz force due to wind, proportional to $\mathbf{U} \times \mathbf{B}$; hence, the Pedersen current is perpendicular to \mathbf{B} , and the Hall current is proportional to $\mathbf{U} \times \mathbf{B} \times \mathbf{B}$, which is $-\mathbf{B}^2 \mathbf{U}^\perp$. Hall currents typically dominate over much of the dynamo region except at its lower and upper edges (Figure 2b). Furthermore, we can quantify the effect of including electron-ion collisions in our treatment: a reduction of Hall and Pedersen conductivities by up to 19% and 75%, respectively (Figure 2b).

Supporting Information S1 also derives currents due to the electric fields, plasma pressure gradients, and gravity force (all calculated in the MHD model). These currents' combined magnitude is $\sim 10\%$ of wind-driven currents. Equation (1) is used to calculate three-dimensional currents above InSight as a function of altitude, local time, and season. We also calculate the magnetic field at the planetary surface due to these currents, making the assumption that the currents are horizontally uniform (i.e., only varying vertically) since (a) the dominant wind patterns simulated by the LMD-MGCM vary on length scales of $\sim 10^\circ$ (corresponding to ~ 600 km) and (b) the currents flow mostly at < 180 -km altitude, that is, the

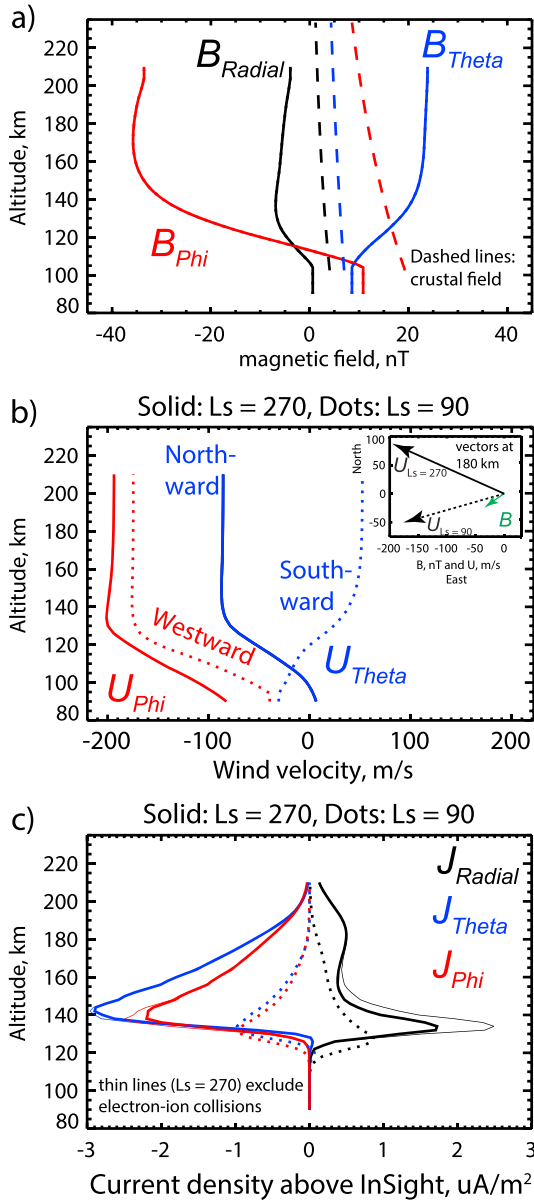


Figure 3. Altitude profiles of (a) magnetic field (solid: total field, dashed: crustal field), (b) winds, and (c) the currents they produce, modeled above the InSight landing site at 2 p.m. local time at northern summer solstice ($L_s = 90^\circ$) and winter solstice ($L_s = 270^\circ$), in spherical polar coordinates. Thin lines in (c) ignore electron-ion collisions for $L_s = 270^\circ$. Inset in (b) are vectors of magnetic field and wind at these two seasons.

contributions of currents from geographically adjacent regions with different wind vectors can be neglected. In addition, in this approximation, only horizontal components of the current system produce fields on the surface. Therefore, in spherical polar coordinates and SI units,

$$B_\phi = \frac{\mu_0}{2} \int_0^\infty J_\theta(z) dr, \quad B_\theta = -\frac{\mu_0}{2} \int_0^\infty J_\phi(z) dr, \quad B_r = 0 \quad (8)$$

where μ_0 is the permeability of free space. Section S2 contains a derivation of the above expressions.

4. Results and Discussion

Let us first examine an example snapshot of the system to demonstrate how magnetic fields and winds interact to produce dynamo currents. Figure 3 shows the system at 2 p.m. local time at both northern summer solstice ($L_s = 90^\circ$) and winter solstice ($L_s = 270^\circ$), showing that the same draped magnetic field pattern (Figure 3a) interacting with neutral winds with different directions (Figure 3b), can result in very different currents. For $L_s = 90^\circ$, the neutral wind is close to parallel to the magnetic field (Figure 3b, inset), meaning that both terms in equation (1) are very small, so the resulting currents are also very small in the horizontal direction (dashed lines in Figure 3c). In contrast, for $L_s = 270^\circ$, the wind has a similar magnitude but makes a significant angle with the magnetic field vector. This results in substantial horizontal current densities, up to $2 \mu\text{A}/\text{m}^2$ around 140-km altitude. A comparison of thin versus thick lines in Figure 3c also shows the degree to which inclusion of electron-ion collisions is necessary to accurately calculate dynamo currents. The largest effect of including these collisions ($\sim 30\%$) is seen for radial currents which do not, in this approximation, produce surface fields, thus the effect on surface fields is on the order of 10%

Figure 4 shows how our modeled dynamo currents, and the resulting surface magnetic fields, vary diurnally and seasonally. As equation (1) implies, currents are primarily determined by the strength of the ionospheric magnetic field, by the strength of the wind components perpendicular to that field, and by the conductivities (equations (2)–(5)), which are proportional to plasma density. Several features in Figure 4 are worth discussing. First, significant currents tend to be a dayside phenomenon due to the weak nightside ionosphere on Mars providing far fewer current carriers. However, it is worth noting that the ionospheric simulations in the Mars Climate Database do not self-consistently calculate the nightside ionosphere, that is, they ignore electron impact ionization, which has been shown to locally increase ionospheric density significantly, though still rarely above 5% of dayside densities (Girazian et al., 2017a; Girazian et al., 2017b; Lillis et al., 2011; Němec et al., 2011; Safaeinili et al., 2007).

Second, the reversal in the eastward component of magnetic field between 09:00 and 10:00 local time is due to the reversal in the magnetic field above InSight discussed in the second paragraph of section 2, that is, the dynamic contest between comparable-strength eastward crustal field and westward draped IMF would not occur for an eastward IMF. Third, current densities tend to be larger in the morning than the afternoon. This is due to typically stronger thermospheric morning winds over the InSight landing site (see Figures 1e and 1f). Fourth, and related to the previous point, larger currents are expected at the solstices compared with equinoxes due to the stronger interhemispheric flow between the winter and summer poles at these times of year. Fifth, currents are the strongest near perihelion ($L_s = 250^\circ$) because (a) stronger winds occur near solstices as just mentioned, (b) winds are driven by stronger solar heating (40% higher than

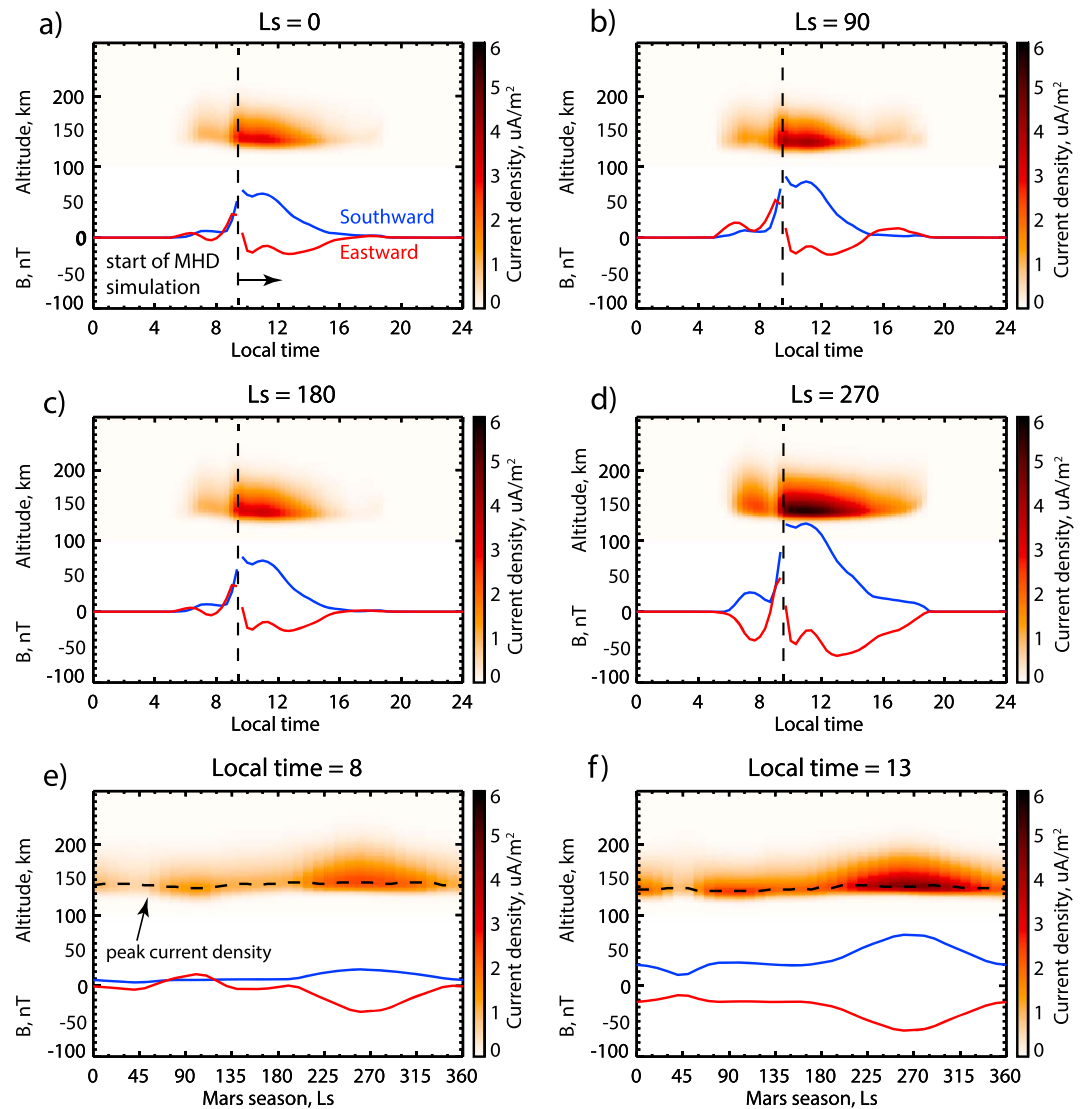


Figure 4. Diurnal and seasonal variability of modeled dynamo current density and resulting surface magnetic fields at the InSight landing site. (a)–(d) show the cardinal seasons ($L_s = 0^\circ, 90^\circ, 180^\circ,$ and 270°). Vertical dashed lines mark the local time on Elysium Planitia when the MHD simulation starts. (e) and (f) show seasonal variation at local times 8:00 and 13:00. Y axes represent both surface magnetic field (blue and red lines for polar and azimuthal components, respectively) and altitude.

aphelion), and (c) higher solar EUV produces greater ionospheric densities and hence conductivities, as is also the case at solar maximum compared with solar minimum. Indeed, CO_2 photoionization frequencies, and hence plasma densities and conductivities, can vary by a factor of ~ 4 over the combination of seasonal and solar cycle variations. Sixth, the peak altitude for currents varies by 10–15 km over the Martian year due to the expansion and contraction of the neutral atmosphere (Figures 4e and 4f). Finally, and as shown also in Figure 3, there are times of day when plasma is available and winds are significant but come close to parallel or antiparallel to magnetic fields and current densities consequently become small, as is seen for $L_s = 90^\circ$ around 2 p.m. local time (Figure 3).

The direction and strength of the predicted magnetic fields at the landing site shown in Figure 4 should not be taken as directly predictive of any kind of average day or year. The direction of currents on a given day, and hence the direction of resulting magnetic fields on the ground, will be dependent not only on the wind patterns as mentioned above but also on the magnetic field draping pattern in the dayside ionosphere and its

interaction with the moderate crustal field above InSight. The strength of the draped field is dependent weakly on the strength of the IMF but mostly on the solar wind dynamic pressure, which is converted to magnetic pressure as the IMF piles up around the conducting obstacle of Mars' ionosphere (e.g., Brain et al., 2010). Both the solar wind pressure (SWP) and the IMF direction at Mars are highly variable (Marquette et al., 2018). During quiet solar periods, SWP is typically steady over a few days, whereas IMF direction changes significantly in less than a day. During disturbed periods of higher solar activity, SWP and IMF direction can change dramatically in hours or less. However, while the current directions react significantly with the direction of the draped field, the current magnitudes do not. The draped field can vary by an order of magnitude in strength (Lillis & Brain, 2013), but the resulting change in current densities is much smaller: multiplying the draped field by 0.3 and 3 results in maximum surface fields just ~15% lower and ~5% higher, respectively. In other words, thermospheric winds are the main drivers of dynamo current magnitudes.

5. Conclusions

We have calculated expected wind-driven dynamo current densities in the thermosphere/ionosphere above the InSight landing site in Elysium Planitia and the resulting surface magnetic fields, using electrodynamic theory and inputs from global models of the Martian thermosphere, ionosphere, and magnetosphere. We have also shown that electron-ion collisions, previously ignored, should be considered. We conclude that magnetic fields of tens of nanotesla and even occasionally >100 nT originating in the dynamo region may be present at the InSight landing site. If (as is hoped) fields caused by the lander itself can be subtracted from the data to a degree of accuracy comparable to tens to 100 nT, fields due to wind-driven dynamo currents should be detectable by the InSight Fluxgate Magnetometer

We have shown that these modeled currents and surface fields primarily depend on plasma densities (caused by solar EUV photoionization) and the strength of the neutral wind component perpendicular to the magnetic field. We have examined their diurnal and seasonal variability, demonstrating that they are a dayside phenomenon, with strongest currents each day typically occurring in the late morning due to stronger winds and each year occurring near perihelion due to both stronger winds from solar heating and higher plasma densities from solar EUV. Lastly, we expect a high degree of variability in the direction but not strength of currents and surface fields due to changes in the draped magnetic field pattern in the dayside ionosphere due to Mars' highly dynamic solar wind and IMF environment.

Data sets

All input data are contained in the supporting information. The MAVEN LPW data used in this study may be downloaded from the Planetary Plasma Interactions node of the Planetary Data System (<https://pds-ppi.igpp.ucla.edu/search/view?f=yes&id=pds://PPI/maven.lpw.calibrated>).

References

- Andersson, L., Ergun, R. E., Delory, G., Eriksson, A. I., Westfall, J., Reed, H., et al. (2015). The Langmuir probe and eaves experiment for MAVEN. *Space Science Reviews*, *195*(1-4), 173–198. <https://doi.org/10.1007/s11214-015-0194-3>
- Banerdt, W. B., & Russell, C. T. (2017). Editorial on: Topical collection on InSight mission to Mars. *Space Science Reviews*, *211*(1-4), 1–3. <https://doi.org/10.1007/s11214-017-0414-0>
- Banfield, D., Rodriguez-Manfredi, J. A., Russell, C. T., Rowe, K. M., Leneman, D., Lai, H. R., et al. (2019). InSight Auxiliary Payload Sensor Suite (APSS). *Space Science Reviews*, *215*(1). <https://doi.org/10.1007/s11214-018-0570-x>
- Benna, M., Mahaffy, P. R., Grebowsky, J. M., Fox, J. L., Yelle, R. V., & Jakosky, B. M. (2015). First measurements of composition and dynamics of the Martian ionosphere by MAVEN's neutral gas and ion mass spectrometer. *Geophysical Research Letters*, *42*, 8958–8965. <https://doi.org/10.1002/2015GL066146>
- Brain, D. A., Bagenal, F., Acuña, M. H., & Connerney, J. E. P. (2003). Martian magnetic morphology: Contributions from the solar wind and crust. *Journal of Geophysical Research*, *108*(A12), 1424. <https://doi.org/10.1029/2002JA009482>
- Brain, D. A., Hurley, D., & Combi, M. R. (2010). The solar wind interaction with Mars: Recent progress and future directions. *Icarus*, *206*(1), 1–4. <https://doi.org/10.1016/j.icarus.2009.10.020>
- Fillingim, M. O. (2018). Ionospheric currents at Mars and their electrodynamic effects. In *Electric Currents in Geospace and Beyond*, (Vol. 235, pp. 445–458). Hoboken, NJ, USA: John Wiley & Sons, Inc. <https://doi.org/10.1002/9781119324522>
- Fillingim, M. O., Lillis, R. J., England, S. L., Peticolas, L. M., Brain, D. A., Halekas, J. S., et al. (2012). On wind-driven electrojets at magnetic cusps in the nightside ionosphere of Mars. *Earth Planets and Space*, *64*(2), 93–103. <https://doi.org/10.5047/eps.2011.04.010>
- Fillingim, M. O., Peticolas, L. M., Lillis, R. J., Brain, D. A., Halekas, J. S., Lummerzheim, D., & Bougher, S. W. (2010). Localized ionization patches in the nighttime ionosphere of Mars and their electrodynamic consequences. *Icarus*, *206*(1), 112–119. <https://doi.org/10.1016/j.icarus.2009.03.005>

Acknowledgments

R. J. L., C. M. F., and L. A. were funded by the NASA MAVEN mission prime contract. M. O. F. was funded by the NASA InSight mission prime contract. F. G. G. was funded by the Spanish National Research Council (CSIC) under intramural project CSIC 201450E022 and acknowledges financial support from the State Agency for Research of the Spanish MCIU through the “Center of Excellence Severo Ochoa” award for the Instituto de Astrofísica de Andalucía-CSIC (SEV-2017-0709). F. F. was funded by the French Centre National De La Recherche Scientifique. We are grateful for comments from Hermann Opgenoorth and an anonymous reviewer, whose comments greatly improved the manuscript.

- Forget, F., Hourdin, F., Fournier, R., Hourdin, C., Talagrand, O., Collins, M., et al. (1999). Improved general circulation models of the Martian atmosphere from the surface to above 80 km. *Journal of Geophysical Research*, *104*(E10), 24,155–24,175. <https://doi.org/10.1029/1999JE001025>
- Girazian, Z., Mahaffy, P., Lillis, R. J., Benna, M., Elrod, M., Fowler, C. M., & Mitchell, D. L. (2017a). Ion densities in the nightside ionosphere of Mars: Effects of electron impact ionization. *Geophysical Research Letters*, *44*, 11,248–11,256. <https://doi.org/10.1002/2017GL075431>
- Girazian, Z., Mahaffy, P. R., Lillis, R. J., Benna, M., Elrod, M., & Jakosky, B. M. (2017b). Nightside ionosphere of Mars: Composition, vertical structure, and variability. *Journal of Geophysical Research: Space Physics*, *122*, 4712–4725. <https://doi.org/10.1002/2016JA023508>
- Gonzalez-Galindo, F., Chaufray, J. Y., Lopez-Valverde, M. A., Gilli, G., Forget, F., Leblanc, F., et al. (2013). Three-dimensional Martian ionosphere model: I. The photochemical ionosphere below 180 km. *Journal of Geophysical Research: Planets*, *118*, 2105–2123. <https://doi.org/10.1002/Jgr.20150>
- Gonzalez-Galindo, F., Forget, F., Lopez-Valverde, M. A., & Coll, M. A. I. (2009). A ground-to-exosphere Martian general circulation model: 2. Atmosphere during solstice conditions—Thermospheric polar warming. *Journal of Geophysical Research*, *114*, E08004. <https://doi.org/10.1029/2008JE003277>
- Heelis, R. A. (2004). Electrodynamics in the low and middle latitude ionosphere: A tutorial. *Journal of Atmospheric and Solar-Terrestrial Physics*, *66*(10), 825–838. <https://doi.org/10.1016/j.jastp.2004.01.034>
- Lillis, R. J., & Brain, D. A. (2013). Nightside electron precipitation at Mars: Geographic variability and dependence on solar wind conditions. *Journal of Geophysical Research: Space Physics*, *118*, 3546–3556. <https://doi.org/10.1002/Jgra.50171>
- Lillis, R. J., Fillingim, M. O., & Brain, D. A. (2011). Three-dimensional structure of the Martian nightside ionosphere: Predicted rates of impact ionization from Mars Global Surveyor magnetometer and electron reflectometer measurements of precipitating electrons. *Journal of Geophysical Research*, *116*, A12317. <https://doi.org/10.1029/2011JA016982>
- Ma, Y. J. (2004). Three-dimensional, multispecies, high spatial resolution MHD studies of the solar wind interaction with Mars. *Journal of Geophysical Research*, *109*, A07211. <https://doi.org/10.1029/2003JA010367>
- Ma, Y. J., Russell, C. T., Fang, X., Dong, C. F., Nagy, A. F., Toth, G., et al. (2017). Variations of the Martian plasma environment during the ICME passage on 8 March 2015: A time-dependent MHD study. *Journal of Geophysical Research: Space Physics*, *122*, 1714–1730. <https://doi.org/10.1002/2016JA023402>
- Ma, Y. J., Russell, C. T., Fang, X., Dong, Y., Nagy, A. F., Toth, G., et al. (2015). MHD model results of solar wind interaction with Mars and comparison with MAVEN plasma observations. *Geophysical Research Letters*, *42*, 9113–9120. <https://doi.org/10.1002/2015GL065218>
- Marquette, M. L., Lillis, R., Halekas, J., Luhmann, J., Gruesbeck, J., & Espley, J. (2018). Autocorrelation study of solar wind plasma and IMF properties as measured by the MAVEN spacecraft. *Journal of Geophysical Research: Space Physics*, *123*, 2493–2512. <https://doi.org/10.1002/2018JA025209>
- Millour, E., Forget, F., & Lewis, S. R. (2017). The Mars Climate Database (MCD version 5.3), 2017/04/1.
- Mittelholz, A., Johnson, C. L., & Lillis, R. J. (2017). Global-scale external magnetic fields at Mars measured at satellite altitude. *Journal of Geophysical Research: Planets*, *122*, 1243–1257. <https://doi.org/10.1002/2017JE005308>
- Němec, F., Morgan, D. D., Gurnett, D. A., & Brain, D. A. (2011). Areas of enhanced ionization in the deep nightside ionosphere of Mars. *Journal of Geophysical Research*, *116*, E06006. <https://doi.org/10.1029/2011JE003804>
- Opgenoorth, H. J., Dhillon, R. S., Rosenqvist, L., Lester, M., Edberg, N. J. T., Milan, S. E., et al. (2010). Day-side ionospheric conductivities at Mars. *Planetary and Space Science*, *58*(10), 1139–1151. <https://doi.org/10.1016/j.pss.2010.04.004>
- Riousset, J. A., Paty, C. S., Lillis, R. J., Fillingim, M. O., England, S. L., Withers, P. G., & Hale, J. P. M. (2014). Electrodynamics of the Martian dynamo region near magnetic cusps and loops. *Geophysical Research Letters*, *41*, 1119–1125. <https://doi.org/10.1002/2013GL059130>
- Safaenili, A., Kofman, W., Mouginot, J., Gim, Y., Herique, A., Ivanov, A. B., et al. (2007). Estimation of the total electron content of the Martian ionosphere using radar sounder surface echoes. *Geophysical Research Letters*, *34*, L23204. <https://doi.org/10.1029/2007GL032154>
- Schunk, R. W., & Nagy, A. (2009). *Ionospheres: Physics, plasma physics, and chemistry*, (2nd ed.). New York: Cambridge Univ. Press. <https://doi.org/10.1017/CBO9780511635342>
- Withers, P., Fallows, K., Girazian, Z., Matta, M., Häusler, B., Hinson, D., et al. (2012). A clear view of the multifaceted dayside ionosphere of Mars. *Geophysical Research Letters*, *39*, L18202. <https://doi.org/10.1029/2012GL053193>
- Withers, P., Mendillo, M., Rishbeth, H., Hinson, D. P., & Arkani-Hamed, J. (2005). Ionospheric characteristics above Martian crustal magnetic anomalies. *Geophysical Research Letters*, *32*, L16204. <https://doi.org/10.1029/2005GL023483>